Phosphorus Adsorption by Red Mud Based Al/Fe-MOFs Synthesized by Ultrasonic-Assisted Solvent Method: Performance and Mechanisms

Hongxi Li[1], Leping Wu[1], Meng Mei[1,3], Tao Gaoliang[2*], Jinping Li[1,3*]

[1]School of Resource and Environment, Wuhan Textile University, Wuhan 430073, China
[2]Key Laboratory of Intelligent Health Perception and Ecological Restoration of Rivers and Lakes, Ministry of Education，Hubei University of Technology, Wuhan 430068, China
[3]Engineering Research Centre for Clean Production of Textile Dyeing and Printing, Ministry of Education, Wuhan Textile University, Wuhan 430073, China

Abstract. Phosphorus (P) removal and the resource utilization of red mud(RM) critical environmental concerns. Red mud as a by-product of alumina production, constitutes a complex mixture of various valuable metals. In this study, a new Al/Fe-MOFs was synthesized using acid-leached RM via ultrasound-assisted solvothermal methods. The adsorption performance and mechanisms of the synthesized materials were systematically investigated. Results indicate that acid leaching of RM significantly enhanced adsorbent efficiency under various pH conditions and in the presence of competing ions. The phosphate adsorption process followed the Pseudo-second-order model and Freundlich models. Mechanistic analysis revealed a synergistic effect, with adsorption proceeding primarily through chemical adsorption and electrostatic interactions through the formation of surface hydroxyl groups.

1 Introduction

Phosphorus (P) is indispensable for the ecosystem, yet its excessive discharge is a primary cause of aquatic eutrophication. Whenphosphorus concentration exceed threshold levels in water bodies,they stimulate excessive aquatic plant growth and water quality deterioration. Thus, the effective removal and subsequent recovery of excess phosphate from aquatic systems have emerged as significant strategies for mitigating resource scarcity and environmental pollution[1]. Excess phosphorus can be removed through various methods, such as biological treatment, adsorption, and chemical precipitation. Among these, adsorption has employed various materials such as activated carbon, zeolites, and organic polymers for phosphate removal[2]. Previous studies indicate thaFe and Al-based materials are particularly effective for adsorbing inorganic oxyanions.

Red mud(RM) is rich in iron and aluminum and has shown potential for phosphate adsorption. Although RM has been utilized in construction materials, agricultural fertilizers, and as an adsorbent, its application in aquatic environments remains limited. In recent years, metal-organic frameworks (MOFs) have gained widespread use as adsorbents for hazardous substances.

In this study, a new Al/Fe-MOFs was successfully synthesized from red mud via an ultrasound-assisted solvothermal method, demonstrating promising potential for phosphate adsorption applications. This study differs from previous studies by avoiding the use of high-purity Fe/Al compounds. Instead, strong acid was employed to activate silicon within red mud, promoting the formation of stable structural frameworks with other components. Concurrently, Fe and Al in the raw material were effectively utilized to synthesize new MOFs and produce efficient adsorption. The adsorption performance of the material was systematically evaluated, with a focus on the remediation of low-concentration phosphorus.The study provides valuable information on the performance of red mud in water pollution control and resource recovery, thereby expanding the application of RM materials in the field of functional MOFs.

2 Materials and methods

2.1. Materials

RM is produced in Shandong, China, particle size less than 0.074 mm. Other chemicals were purchased from China National Pharmaceutical Group Chemical Reagent Co.

2.2 Preparation of various adsorbents

RM was mixed with 4 M HCl at a solid-to-liquid ratio of 1:10 (g/mL)and stirred at room temperature for 2 hours. The resulting solid was dried at 105°C to constant weight, yielding the precursor designated as RM-Cl. Subsequently, 0.3 g of 1,4-dicarboxybenzene was

*Jinping Li: lijinping@wtu.edu.cn

dissolved in 30 mL of N,N-dimethylformamide(DMF). Then, 0.5 g of RM-Cl was added to this solution, and the mixture was sonicated for 15 minutes. The mixture was transferred to a hydrothermal reactor and heated at 110°C for 24 hours. After the reaction, the solid product was collected by centrifugation, repeatedly washed with deionized water until the supernatant exhibited no observable change, and finally dried at 85°C to obtain the material designated as Al/Fe-Cl. Using the same procedure, Al/Fe-N and Al/Fe-S were synthesized with nitric acid and sulfuric acid, respectively.

2.3 Characterization

SEM, ZEISS GeminiSEM 300. XRD, Rigaku SmartLab SE. FTIR, Thermo Fisher Scientific Nicolet iS20. XPS, Thermo Scientific K-Alpha.

3 Results and discussion

3.1. Micromorphology

The SEM-EDS results of Al/Fe-X are shown in Figure 1. Al/Fe-O exhibited an irregular porous structure composed of columnar crystals approximately 250 nm in size.. In contrast, the acid-leached samples (Al/Fe-X) displayed larger overall volumes and higher specific surface areas, consisting of smaller particles. Specifically, Al/Fe-Cl and Al/Fe-N featured surface pore sizes exceeding 300 nm, with some pores in Al/Fe-Cl larger than 1000 nm. Meanwhile, Al/Fe-S formed distinctive tubular crystals with diameters around 500 nm[3].

The XRF results of RM are shown in Table 1. According to the XRD analysis, Fe and Al species acted as the main reactive components during synthesis, while Si provided a stable structural support. Although RM has a complex and variable composition, the synthesis method used in this study was not significantly affected by these variations.

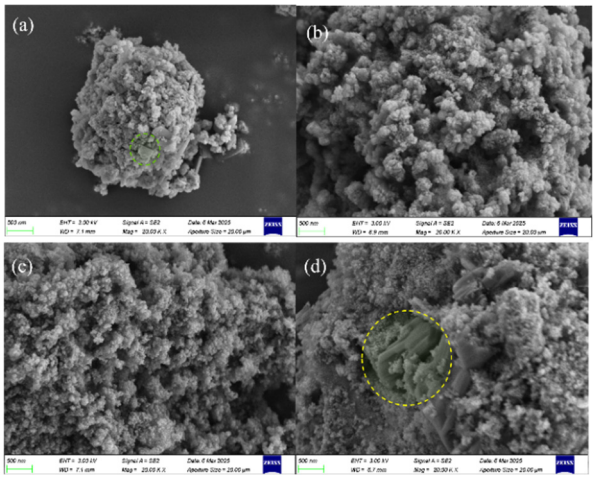

Fig. 1. SEM results of (a) Al/Fe-O; (b) Al/Fe-Cl; (c) Al/Fe-N; (d) Al/Fe-S.

Table 1. Compositional matrix of the RM.

Compound Formula	Wt. Percent (%)
Fe_2O_3	36.795
Al_2O_3	22.379
SiO_2	16.078
Na_2O	11.696
TiO_2	5.592
CaO	5.538
K_2O	0.305
ZrO_2	0.284
MgO	0.273
SO_3	0.266
V_2O_5	0.246
P_2O_5	0.207

3.2 BET and XRD analysis

The adsorption/desorption experiment result shown in Fig.2a-b, as classified by the IUPAC, suggests the presence of a combination of mesopores in sepiolite and along with narrow slit pores. Meanwhile, the average pore size changes from 90.882 nm (Al/Fe-O) to 45.134 nm-61.306 nm (Al/Fe-X), and with the change in acid treatment, the pore volume also increased. It shows that the acid leaching significantly changed the specific surface areas of the materials. The Al/Fe-S exhibited the highest surface area (324.99 m^2/g), indicating that sulfuric acid leaching effectively optimized pore structures. However, the Al/Fe-Cl decreases in the surface area but the adsorption capatial has not changed, instead of the adsorption capatial is still higher than Al/Fe-O. These might be a reason that during the synthesis of Al/Fe-X, ultrasonic waves dispersed Cl- within the pores of the Al/Fe-Cl, leading to partial blockage. Nevertheless, it facilitates the transfer of phosphate on its surface.

The crystal structure of Al/Fe-X results are shown in Figure 2b. The XRD pattern of Al/Fe-X exhibits characteristic peaks at 2θ = 29.41°, 35.96°, 39.40° and 43.15°, corresponding to Fe_2O_3 (PDF#39-1346). Additional peaks at 2θ = 20.86° and 26.64°, which can be attributed to SiO_2 (PDF#99–0088). The XRD pattern of the reference material Al/Fe(0.5) displays peaks at 2θ = 6.85°, 19.92°, 24.91°, 27.27°and 28.28°. The observed diffraction peaks are sharp and exhibit similar profiles, indicating that the Al/Fe-X materials possess a crystal structure analogous to that of Al/Fe(0.5) [4].

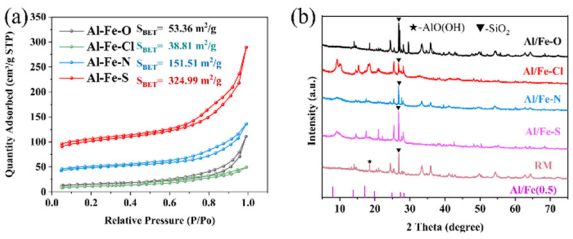

Fig. 2. (a) N_2 adsorption-desorption isotherms; (b) XRD patterns.

3.3 Adsorption kinetic

The change in phosphate concentration over time during adsorption by Al/Fe-X in Figure 3a. Kinetic studies

indicated that Al/Fe-X exhibited superior phosphate adsorption performance compared to Al/Fe-O in terms of adsorption rate and maximum capacity. Initially, the adsorption process proceeded rapidly, which can be attributed to the abundance of available active sites and favorable surface properties. As adsorption continued, the phosphate concentration in solution gradually decreased. Concurrently, the active sites became progressively saturated, eventually reaching adsorption equilibrium. Moreover, the adsorption kinetics of Al/Fe-X appear to be predominantly governed by its surface structure and the distribution of active sites.

Table 2. Fitting results of isotherm parameters.

Models	Parameters	Al/Fe-S		
Langmuir	q_{max}	298K	308K	318K
	k_L	92.02	139.48	75.59
	R_L	0.026	0.045	0.050
	R^2	0.6922	0.5813	0.9214
Freundlich	1/n	0.89	0.94	0.92
	K_F	0.623	0.532	0.507
	R^2	4.7661	7.9591	12.956
Thermody-namic	ΔH	0.928	0.980	0.964
	ΔS	39.393		
	ΔG	0.145		

3.4 Adsorption isotherm and thermodynamic

As shown in Table 2 and Figure 3b, the Freundlich model provided a better fit compared to the Langmuir model, indicating heterodisperse adsorption surfaces. This heterogeneity likely originates from the non-uniform distribution of active sites, which can be attributed to impurities in the precursor materials. When the temperature increased to 318 K, the phosphate adsorption capacity of Al/Fe-X improved, confirming that a positive temperature dependence. These associated changes reflect alterations in the solid-liquid interface arrangement due to the movement and binding of phosphate ions.

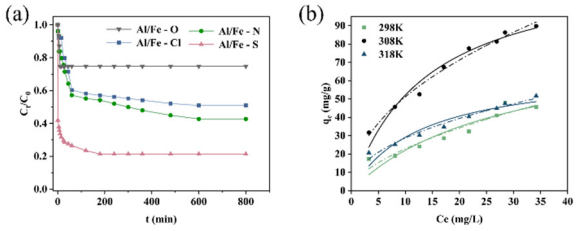

Fig. 3. (a)Adsorption kinetics of different absorbents; Adsorption at different temperatures (b) Al/Fe-S. The solid line and dashed line are the Langmuir model and Freundlich model.

3.5 Influence of initial pH and coexisting ions

As shown in Figure 4b, within the pH range of 4.0 to 7.2, the dominant phosphates in the solution were HPO_4^{2-} and H_2PO^{4-} , both of which were readily adsorbed. When pH was below 3.0, structural alteration of the adsorbent occurred, which further reduce adsorption. When pH exceeded 4.0, phosphate ions competed with -OH for active sites, reduce adsorption efficiency. When the pH exceeded 8.0, the surface hydroxyl groups of Al^{3+} containing active sites generated electrostatic repulsion due to deprotonation, which inhibited phosphate adsorption[5].

The coexisting ions could significantly influenced phosphate adsorption, as presented in Figure 4b. Al/Fe-S was more susceptible to interference from coexisting ions, whereas certain ions exhibited a cooperative effect on phosphate adsorption for Al/Fe-Cl and Al/Fe-N. These results indicate that acid leaching enhances the adsorbent stability and phosphate selectivity under realistic aqueous conditions.

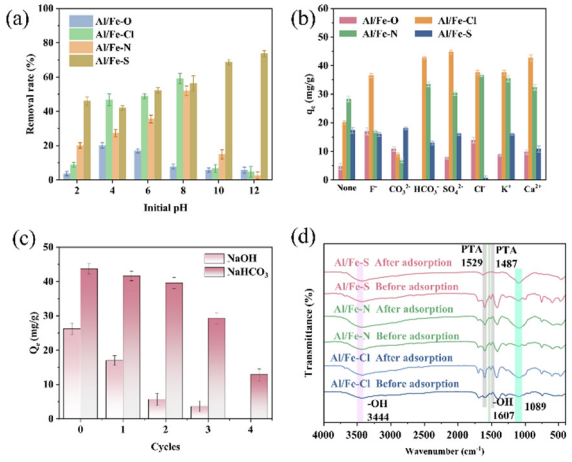

Fig. 4. (a) The influence of initial pH(b) The influence of coexisting ions (c)The recycling of Al/Fe-S(d) FTIR spectra.

3.6 Adsorbent cycles

The cycle test results of Al/Fe-S shown in Figure 4c. After three adsorption-desorption cycles, its phosphate adsorption capacity retained only 13.86% of the initial value. However, when regenerated with $NaHCO_3$, the material maintained 29.5% of its original capacity after four cycles. This decline is primarily attributed to the cumulative loss of metal adsorption sites during regeneration, which reduces phosphate binding efficiency. These results suggest that Al/Fe-X materials exhibit limited reusability in alkaline aqueous environments[4].

3.7 Adsorption mechanism

The adsorption mechanism was further analyzed by FTIR and XPS. The change in FTIR spectra of Al/Fe-X before and after phosphate adsorption are presented in Figure 4d. The wavenumber at 3444 cm^{-1} is assigne to the stretching vibration of surface -OH groups. After adsorption, the characteristic peak of Al/Fe-S shifted from 1626 cm^{-1} to 1627 cm^{-1}, which corresponds to hydroxyl bending vibrations. The peak at 1099 cm^{-1} is associated with aldol condensation involving surface oxhydryl groups. Additionally, the appearance of a peak at 531 cm^{-1} is attributed to asymmetric bending vibrations of O=P-O bonds[6]. The peak at 1607 cm^{-1} indicates the stretching vibration of the -OH group in adsorbed H_2PO^{4-}. These

results confirm that chemical adsorption is the dominant mechanism for phosphate removal by Al/Fe-X.

The XPS spectra of Al/Fe-X are shown in Figure 5. The appearance of the distinct P 2p peak in the wide scan spectrum after adsorption confirmed the successful adsorption of phosphate. Notably, the P 2p binding energies for Al/Fe-Cl and Al/Fe-N are consistent with those for P adsorbed on magnetite (134.01eV) and ferrihydrite (133.95eV) via inner-sphere complexation[6]. The increase in Fe 2p binding energy after adsorption suggests electron transfer and supports the formation of Fe-O-P inner-sphere complexes. In Al/Fe-Cl, a decrease in binding energy and the disappearance of the peak near 717eV further indicate electron transfer involving Fe(III)[7]. The Fe 2p spectra also exhibited mixed Fe(II)/Fe(III) characteristics. Furthermore, an increase in Al 2p binding energy was observed, indicating electron transfer within the valence bands and the formation of Al–O–P inner-sphere complexes during adsorption.

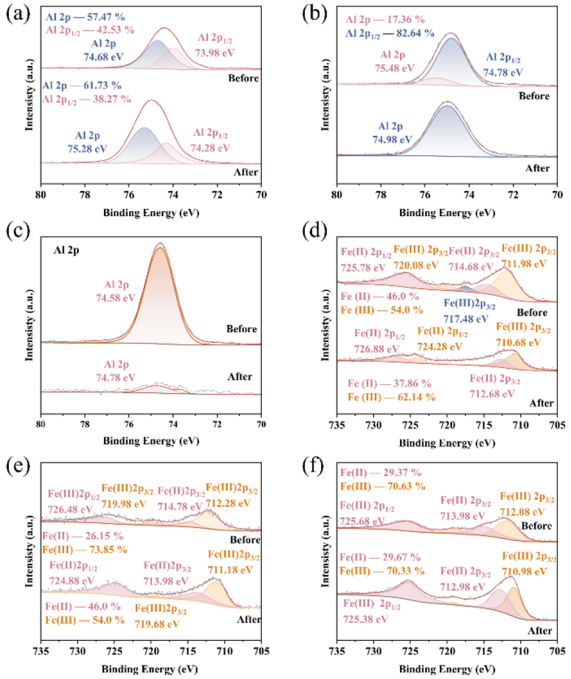

Fig. 5. (a) Al/Fe-Cl (b) Al/Fe-N (c) Al/Fe-S; XPS spectra of Fe2p (d) Al/Fe-Cl (e) Al/Fe-N (f) Al/Fe-S.

4 Conclusions

This study developed a novel Al/Fe based MOFs (Al/Fe-X) derived from red mud via a low-cost ultrasound-assisted solvent method. The synthesized adsorbent exhibited high phosphate adsorption capacity. Acid leaching significantly improved the adsorption performance, with sulfuric acid treatment yielding the highest capacity. The analysis results indicated that phosphate adsorption on Al/Fe-X primarily through ligand exchange at metal active sites. These findings present a viable strategy for integrating phosphorus removal with the resource utilization of red mud, offering both theoretical insight and practical guidance for solid waste management and wastewater treatment.

Acknowledgement

This work was supported by the National Natural Science Foundation of China (Nos.51208393), and the Open Project Funding of Key Laboratory of Intelligent Health Perception and Ecological Restoration of Rivers and Lakes, Ministry of Education, Hubei University of Technology. The authors would also like to thank all the reviewers who provided comments on this paper.

References

1. Chen T P., Feng T., Wu S, et al. 2025, MOF-derived FeCe@Carbon catalysts for the efficient tetracycline degradation by activated persulfate: Preparation and mechanistic study. Journal of Colloid and Interface Science, 685: 1041-1055. https://doi.org/10.1016/j.jcis.2025.01.203.
2. Zhang T., Li J., Liu D, et al. 2025, Constructing a low-cost total Ce (III)-based adsorbent for efficient removal and recovery of phosphate. 505: 159516. https://doi.org/10.1016/j.cej.2025.159516.
3. Zhang T., Li J L., Liu D Q, et al. 2025, Constructing a low-cost total Ce(III)-based adsorbent for efficient removal and recovery of phosphate. Chemical Engineering Journal, 505. https://doi.org/10.1016/j.cej.2025.159516.
4. Li S., Lei T., Jiang F, et al. 2020, Tuning the morphology and adsorption capacity of Al-MIL-101 analogues with Fe^{3+} for phosphorus removal from water. Journal of Colloid and Interface Science, 560: 321-329. https://doi.org/10.1016/j.jcis.2019.10.077.
5. Zhou G., Yang S., Sun Y, et al. 2025, Adsorption process and mechanism analysis of porous ZnO@MIL-101(Cr) composites prepared by a convenient hydrothermal method for efficiently removing hydrogen sulfide. Separation and Purification Technology: 133849.https://doi.org/10.1016/j.seppur.2025.133849
6. Li X., Li L., Zhang Z, et al. 2025, Insights into the mechanism of mechanically treated Fe/Mn-N doped seed meal hydrochar for efficient adsorption and degradation of tetracycline. Biochar, 7(1): 48.10.1007/s42773-025-00435-5.
7. Shen C., Dong X., Yang J, et al. 2025, Red mud-based magnetic biochar composite as a peroxydisulfate activator for tetracycline degradation. Environmental Research, 279: 121793.https://doi.org/10.1016/j.envres.2025.121793.